Double Coaxial Structure and Dual Physicochemical Properties of Carbon Nanotubes Composed of Stacked Nitrogen-Doped and Undoped Multiwalls

Quanhong Yang, Weihua Xu, Akira Tomita, and Takashi Kyotani*

Institute of Multidisciplinary Research for Advanced Materials, Tohoku University, 2-1-1 Katahira, Sendai 980-8577, Japan

Received December 13, 2004. Revised Manuscript Received March 9, 2005

Carbon nanotubes with a double coaxial structure of nitrogen-doped and undoped multiwalls were successfully prepared by the template technique using porous anodic aluminum oxide film as a template. The inner carbon layer (or the outer carbon layer) of the double coaxial carbon nanotubes is free from N, while the outer carbon layer (or the inner carbon layer) is uniformly doped with N. Transmission electron microscopy cannot differentiate between the outer and inner layers, but all the results by Raman, X-ray diffraction, and X-ray photoelectron spectroscopy provide evidence that the N-doped layer is less crystallized than the undoped one. Furthermore, the N-doped layer has apparently higher chemical reactivity toward oxygen than the undoped one due to more edge-active sites resulting from the introduction of nitrogen species. Electrical conductance measurement indicates that despite poorer crystallinity the N-doped layer has higher conductivity than undoped one. The resulting multiwalled carbon nanotubes thus have not only double-stack coaxial structure but also dual physicochemical properties.

1. Introduction

Carbon nanotubes (CNTs) have excellent electrical, mechanical, and physicochemical properties, especially, electrical characteristics being sensitively dependent on the diameter and helix of nanotubes.[1] However, regrettably, no one has been able to precisely control these structural parameters up to date.[2] Doping of heteroatoms into rolled graphene layers constituting CNTs is believed to be another way to effectively adjust the electronic conductance characteristics and other properties.[3] Many kinds of doped CNTs have been prepared so far.[4] Nitrogen-doped CNTs are predicted to be potential *n*-type semiconductors and have been synthesized in many ways such as thermal chemical vapor deposition (CVD) of N-containing organic compounds in the presence of metal catalysts,[5−11] hot filament CVD of $N_2-CH_4-NH_3$,[12,13] electron cyclotron resonance CVD of the mixture of C_2H_2 and N_2,[14] and magnetron sputtering of a graphite target under Ar/N_2.[15] In some of these works, N distribution in the N-doped CNTs was investigated. However, effective control of N location and distribution in the doped nanotubes is still a big problem. The present group successfully fabricated the CNTs with a double coaxial structure of N-doped and undoped multiwalls using the template technique for the first time. The synthesis of such nanotubes was briefly reported in a short communication where it has been proved that the prepared nanotubes are characterized by the inner (or outer) N-doped and outer (or inner) undoped layers.[16]

The present study reports the details of the double coaxial structure of the novel CNTs and discusses the difference in structure and properties between the coaxial N-doped and undoped layers in the following aspects: N distribution, microscopic features, crystallinity, chemical reactivity, and electrical conductance performance. It has been demonstrated that the template technique is very effective to intentionally synthesize CNTs with controllable structure (size, heteroatom distribution) and adjustable properties, which is of great importance for fabricating the real CNT-based nanodevices.

* Corresponding author. E-mail: kyotani@tagen.tohoku.ac.jp.

(1) Dresselhause, M. S.; Dresselhause, G.; Eklund, P. C. *Science of Fullerenes and Carbon Nanotubes*; Academic Press: San Diego, 1996.
(2) Dai, H. J. *Surf. Sci.* **2002**, *500*, 218.
(3) Saito S. *Science* **1997**, *278*, 77.
(4) Terrones, M.; Grobert, N.; Terrones, H. *Carbon* **2002**, *40*, 1665.
(5) Yudasaka, M.; Kikuchi, R.; Ohki, Y.; Yokomura, S. *Carbon* **1997**, *35*, 195.
(6) Suenaga, K.; Yudasaka, M.; Colliex, C.; Iijima, S. *Chem. Phys. Lett.* **2000**, *316*, 365.
(7) Sen, R.; Satishkumar, B. C.; Govindaraj, A.; Harikumar, K. R.; Raina, G.; Zhang, J. P.; Cheetham, A. K.; Rao, C. N. R. *Chem. Phys. Lett.* **1998**, *287*, 671.
(8) Nath, M.; Satishkumar, B. C.; Govindaraj, A.; Vinod, C. P.; Rao, C. N. R. *Chem. Phys. Lett.* **2000**, *322*, 333.
(9) Terrones, M.; Redlich, P.; Grobert, N.; Trasobares, S.; Hsu, W. K.; Terrones, H.; Zhu, Y. Q.; Hare, J. P.; Reeves, C. L.; Cheetham, A. K.; Rühle, M.; Kroto, H. W.; Walton, D. R. M. *Adv. Mater.* **1999**, *11*, 655.
(10) Terrones, M.; Terrones, H.; Grobert, N.; Hsu, W. K.; Zhu, Y. Q.; Hare, J. P.; Kroto, H. W.; Walton, D. R. M.; Kohler-Redlich, P.; Rühle, M.; Zhang, J. P.; Cheetham, A. K. *Appl. Phys. Lett.* **1999**, *75*, 3932.
(11) Terrones, M.; Ajayan, P. M.; Banhart, F.; Blasé, X.; Carroll, D. L.; Charlier, J. C.; Czerw, R.; Foley, B.; Grobert, N.; Kamalakaran, R.; Kohler-Redlich, P.; Rühle, M.; Seeger, T.; Terrones, H. *Appl. Phys. A* **2002**, *74*, 355.
(12) Kurt, R.; Klinke, C.; Bonard, J. M.; Kern. K.; Karimi, A. *Carbon* **2001**, *39*, 2163.
(13) Kurt, R.; Karimi, A.; Hoffmann, V. *Chem. Phys. Lett.* **2001**, *335*, 545.
(14) Sung, S. L.; Tsai, S. H.; Tseng, C. H.; Chiang, F. K.; Liu, X. W.; Shih, H. C. *Appl. Phys. Lett.* **1999**, *74*, 197.
(15) Suenaga, K.; Jahansson, M. P.; Hellgren, N.; Broitman, E.; Wallenberg, L. R.; Colliex, C.; Sundgren, J. E.; Hultman, L. *Chem. Phys. Lett.* **1999**, *300*, 695.
(16) Xu, W. H.; Kyotani, T.; Pradhan, B. K.; Nakajima, T.; Tomita, A. *Adv. Mater.* **2003**, *15* (13), 1087.

10.1021/cm047830m CCC: $30.25
Published on Web 04/12/2005

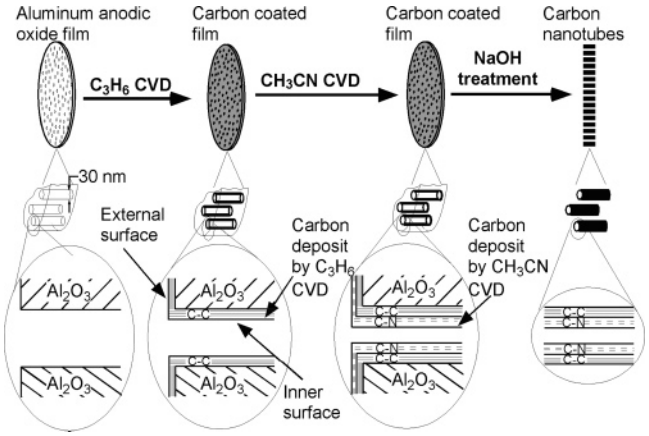

Figure 1. Schematic illustration of the synthesis of the double coaxial CNTs with inner N-doped and outer undoped multiwalls (PA-CNT).[16]

2. Experimental Section

2.1. Materials. By the anodic oxidation of an aluminum plate, an anodic aluminum oxide film (AAO) with a channel diameter of 30 nm and a thickness of about 70 μm was prepared, and details are given elsewhere.[17,18] The resulting AAO film was placed on a quartz boat in a horizontal quartz reactor (inside diameter, 55 mm) and subjected to two-step CVD to prepare double-stack CNTs with controlled N distribution. As shown in the schematic diagram (Figure 1) for preparing CNTs with double coaxial structure, the first propylene CVD (propylene 1.2% in N_2 at a flow rate of 1000 cm^3 (STP)/min) was conducted at 800 °C for 2 h, leading to a uniform coating of a pure carbon layer on the inner wall of the AAO nanochannels. A second CVD was then carried out on the carbon-coated AAO film under an acetonitrile (4.2% in N_2 at a flow rate of 500 cm^3 (STP)/min) vapor flow at 800 °C for 5 h. The latter CVD process gave rise to an N-doped carbon layer on the already-deposited pure carbon layer, leading to the formation of the double structure of N-doped and undoped carbon layers on the inner wall of the nanochannels. Such doubly carbon-coated AAO is denoted as PA/AAO (hereafter, P and A represent propylene and acetonitrile, respectively). After the CVD processes, the carbon-coated AAO film was treated with 10 N NaOH solution at 150 °C for 6 h to remove the AAO template, thereby liberating the nanotubes from the template AAO film. Since the acetonitrile CVD follows the propylene one, the CNTs thus prepared have a double structure of outer undoped and inner N-doped multiwalls (hereafter referred to as PA-CNT).

With a reverse in the CVD sequence, the double coaxial CNTs of outer N-doped and inner undoped multiwalls were prepared. The carbon-coated AAO and resulting CNT are denoted as AP/AAO and AP-CNT, respectively. The one-step propylene CVD over AAO produced single-stack undoped CNTs, and the carbon-coated AAOs and resulting CNTs are referred to as P/AAO and P-CNT. Likewise, the one-step acetonitrile CVD led to N-doped CNTs, and the carbon-coated AAOs and resulting CNTs are denoted as A/AAO and A-CNT, respectively. For any CVD processes, propylene and acetonitrile were introduced into the CVD furnace under the same conditions (concentration and flow rate) as in the PA-CNT case.

2.2. Characterizations. The carbon-coated AAO films and the corresponding CNTs were characterized by several means. Microscopic observation of the samples was performed by field-emission scanning electron microscopy (FESEM, JEOL SM71010) and transmission electron microscopy (TEM, JEOL JEM-2010). Raman spectra were measured using a micro-Raman apparatus (Seishin) with Ar ion laser excitation at 514.5 nm. X-ray diffraction (XRD) measurements were conducted using an X-ray diffractometer (XD-D1, Shimadzu) with Cu Kα radiation. X-ray photoelectron spectroscopy (XPS) measurements were conducted using an ESCA spectrometer (PHI 5600 ESCA, Perkin-Elmer), where a binding energy correction was made to account for sample charging based on the Ag 3d peak at 367.9 eV. Element concentration depth profiles were obtained by XPS with argon sputter etching technique (argon ion beam irradiation under an electric voltage of 1 kV).

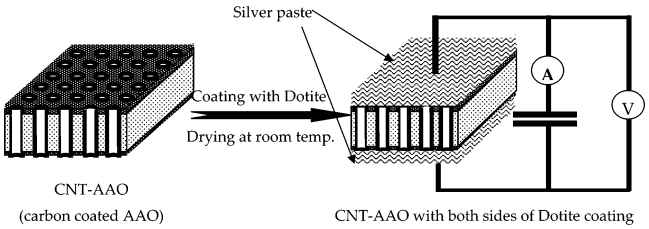

Figure 2. Schematic diagram of electrical conductance measurement of template-synthesized CNTs.

2.3. Oxygen Chemisorption. Oxygen chemisorption measurement was conducted by the following procedure. Each CNT sample was heat-treated under a He flow at 800 °C for 1 h in order to clean the sample surface and then subjected to an O_2 flow at 200 °C (20 cm^3/min of O_2 and 80 cm^3/min of He), followed by a temperature programmed desorption (TPD) measurement (raising temperature from 200 to 1000 °C at a linear heating rate of 10 °C/min under a He flow and then keeping constant at 1000 °C for 30 min). CO_2 and CO gases liberated from the CNTs were quantitatively monitored by a high-speed gas chromatograph.

2.4. Electrical Conductance Measurement. The electrical conductance of the carbon-coated AAO films (CNT-AAO composites) was measured by a two-terminal method as shown in Figure 2. All the nanotubes prepared by the template technique were embedded in the nanochannels of AAO templates and parallel to each other as a result. We coated both sides of a CNT-AAO composite film with silver paste (Dotite 550, Fujikura Kasei), to which two silver wires are attached. A potential (−1.0 to 1.0 V) is applied to both surfaces of the film through the two conducting wires, and the I−V characteristics were measured at a temperature of 25 °C. According to the I−V curves, the resistances were obtained and then the specific resistivity of the prepared CNTs was induced. For each case, five samples were measured to obtain the average resistance (R_m, after the error correction by subtracting the contact resistance of conducting wires and silver paste). The area (denoted as A) of each side of CNT-AAO film employed is about 0.5 cm^2, and the number (n) of nanotubes in an AAO template per unit area is estimated as $5 \times 10^{10}/cm^2$ according to the SEM observation. Apparently, the resistance (R) of an individual nanotube is determined from R_m, n, and A by the equation: $R = nAR_m$. Then the specific resistivity (ρ) of CNT is calculated according to the equation: $\rho = RS/L$ (S and L are the cross-sectional area and length of an individual CNT, respectively).

3. Results

3.1. N Distribution Depth Profile. In the previous study,[16] elemental analyses (bulk N/C ratios) and XPS measurement (surface N/C ratios) provided evidence that the two-step CVD leads to the formation of CNTs with a double coaxial structure with N-doped and undoped multiwalls. The first two columns of Table 1 present a concise summary of elemental analysis and XPS results of carbon-coated AAO and CNTs. In the cases of XPS, the previous communica-

(17) Kyotani, T.; Tsai, L.; Tomita, A. *Chem. Mater*. **1995**, *7*, 1427.
(18) Kyotani, T.; Tsai, L.; Tomita, A. *Chem. Mater*. **1996**, *8*, 2109.

Table 1. Microstructural Parameters and Properties of the Carbon-Coated AAO and Resultant CNTs

			Raman	XRD		XPS	TPD		
sample	bulk N/C ratio	surface N/C ratio	$\Delta\nu_G$[a] (cm^{-1})	L_c[b] (nm)	d_{002}[c] (nm)	fwhm[d] (eV)	CO_2 (μmol/g)	CO (μmol/g)	ρ[e] (Ω·cm)
P-CNT			100	4.0	0.34	1.86	88	36	$(1.6 \pm 0.3) \times 10^3$
PA/AAO		0.056				2.10			
PA-CNT	0.030	0.009	170	2.8	0.35	1.80	262	57	$(1.8 \pm 0.2) \times 10^2$
A-CNT	0.080	0.074	250	2.0	0.36	2.06	600	192	$(2.2 \pm 0.3) \times 10$
AP/AAO		0.012				1.80			
AP-CNT	0.033	0.043	160	3.0	0.35	2.02	325	60	$(2.1 \pm 0.3) \times 10^2$

[a] fwhm of G band in Raman spectra. [b] The crystalline size determined from the (002) peak width using the Scherrer equation. [c] Interlayer distance between graphene planes. [d] fwhm of the sp^2 carbon peaks in XPS. [e] The specific electrical resistivity.

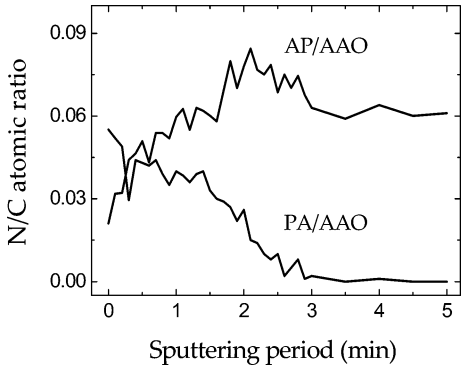

Figure 3. Profiles of N/C atomic ratio of the doubly coated AAO films plotted as a function of argon sputtering time.

tion[16] stated that the obtained spectra mainly reflect the information of the outer layer of the CNTs and are hard to reflect the information of the inner layer, since the escape depth of photoelectrons in XPS is usually 1−3 nm for carbon materials. In the case of the template-synthesized nanotubes, however, the characteristics of their inner surface (inner layer) can be estimated from the analysis of the external surface of the corresponding carbon-coated AAO film as judged from Figure 1. We thus regard an XPS spectrum of each coated AAO film as that of the inner surface (inner layer) of the corresponding nanotubes. By comparison of the surface N/C ratios of carbon-coated AAO (inner surface of CNT) with those of the resultant CNTs (outer surface of CNT) as shown in Table 1, it is easy to conclude that PA-CNT is composed of the outer undoped and inner N-doped multiwalls while AP-CNT is, in the reverse case, of the outer N-doped and inner undoped multiwalls.

The depth profiles of N distribution for the carbon-coated AAO films (PA/AAO and AP/AAO) were analyzed by XPS with the argon sputtering technique. In Figure 3, the N/C atomic ratios of PA/AAO and AP/AAO are plotted as a function of argon sputtering time, which is roughly proportional to the etching depth. For PA/AAO, the N/C atomic ratio decreases with the etching of the upper layer, and after about 3 min sputtering, the N concentration decreases to zero. The N/C atomic ratio profile of AP/AAO is the complete opposite to that of PA/AAO, and the N/C atomic ratio increases during the first 2 min of etching.

3.2. SEM Observation. Parts a and b of Figure 4 show the SEM images of PA-CNT. All the nanotubes exist in bundles of a uniform length of 70 μm, exactly the same as the thickness of the AAO film used as a template. Figure 4b shows the image of ends of the nanotube bundles, and it is demonstrated that the bundled nanotubes are connected to each other by a carbon film that is deposited on the outer surface of AAO in the CVD. The carbon film is retained when the AAO template is removed. Three other kinds of CNTs show an appearance similar to PA-CNT.

3.3. HRTEM Observation. Figure 5 shows high-resolution TEM (HRTEM) images of the wall structure of PA-CNT (a) and AP-CNT (b). The two images show that both samples contain many roughly parallel graphene sheets. However, for each nanotube, these sheets hardly stretch through its entire tube, and the size of most sheets is in the range of 5−10 nm. As a result, significant lattice distortions and defects are observed in the wall structure. All these microscopic features clearly indicate low crystallinity of the present double coaxial CNTs. For both types of double

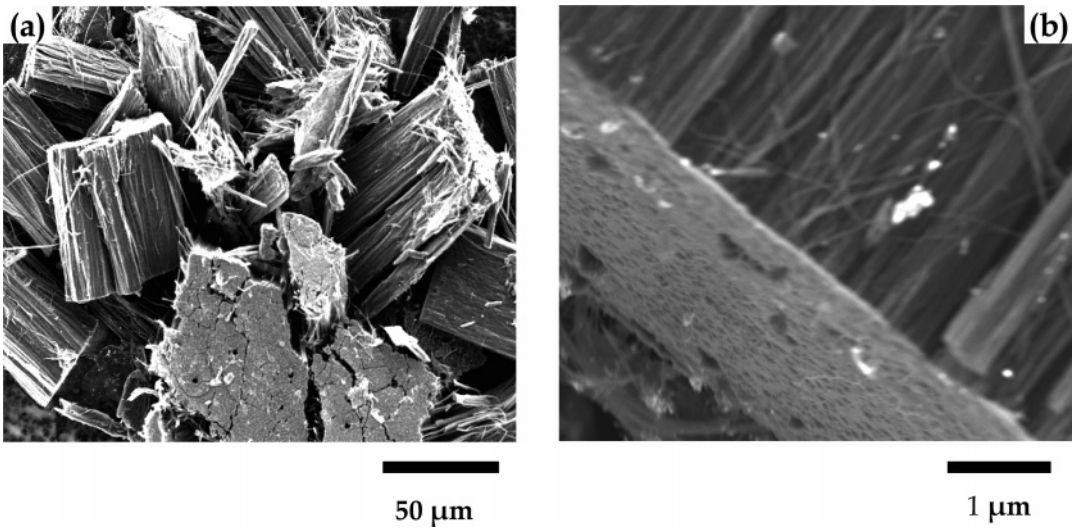

Figure 4. SEM images of PA-CNT. Bundled CNTs (a) and ends of bundled CNTs (b).

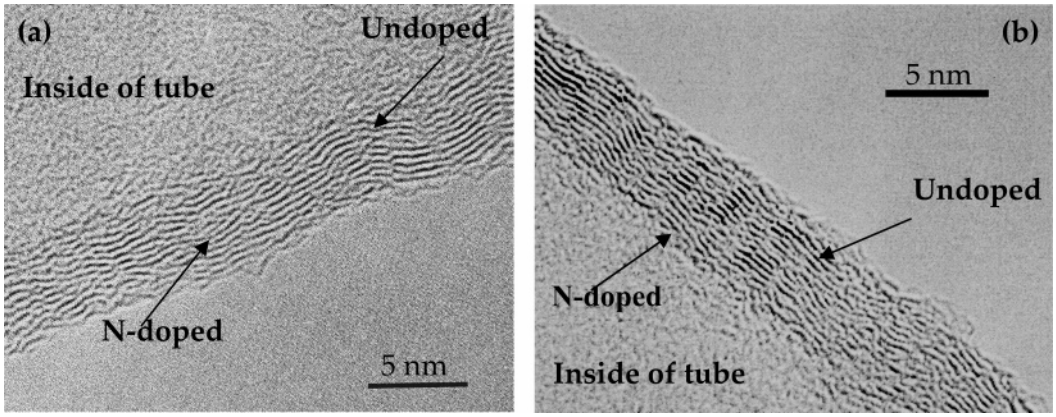

Figure 5. HRTEM images of the tube walls of the AP-CNT (a)[16] and PA-CNT (b).

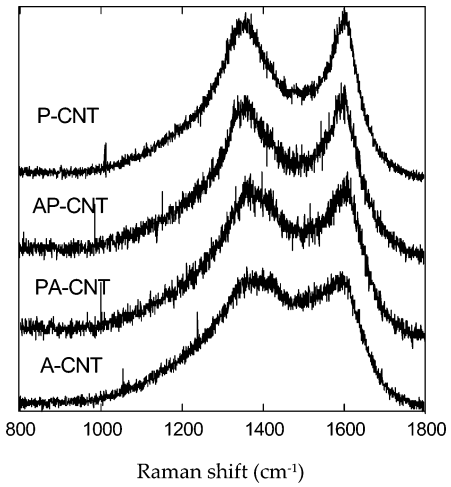

Figure 6. Raman spectra of the double coaxial CNTs and the single-stack CNTs.

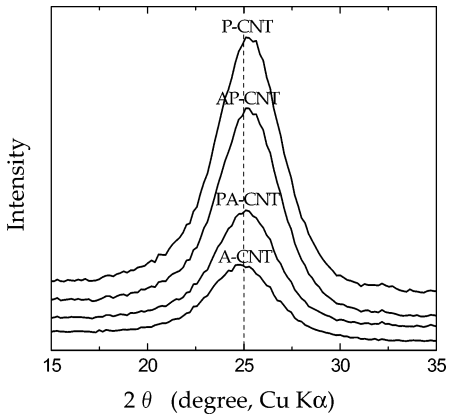

Figure 7. XRD (002) diffraction patterns of the double coaxial CNTs and the single-stack CNTs.

coaxial CNTs, we cannot find any clear interface between the outer and inner layers, and also it is difficult to identify apparent microscopic differences between these two types of double coaxial CNTs.

3.4. Raman Spectra. For the double coaxial CNTs and single-stack CNTs, their Raman spectra (Figure 6) show two weak peaks assigned to the disorder-induced band, the D band, around 1350 cm^{-1}, and the tangential modes, the G band, around 1600 cm^{-1}. This suggests structural imperfection of the rolled graphene sheets. It should also be noted that the G bands of all four samples are upshifted compared with that of graphite (1580 cm^{-1}). It is also demonstrated in Figure 6 that the four samples have apparent differences in the shape of Raman bands and the $\Delta\nu_G$ value (full width at the half maximum (fwhm) of the G band, shown in Table 1). For P-CNT, the two bands are well separated and $\Delta\nu_G$ (100 cm^{-1}) is the lowest in all four samples. Among the four samples, A-CNT has the weakest response for both bands and the largest $\Delta\nu_G$ of 250 cm^{-1}, and moreover, the two bands are greatly overlapped. PA- and AP-CNT have a similar Raman response, and the $\Delta\nu_G$ values are 170 and 160 cm^{-1}, respectively, between P- and A-CNT.

3.5. XRD Pattern. XRD measurements were conducted for the double coaxial and single-stack CNTs, and Figure 7 shows the XRD patterns around the (002) diffraction peak. All four samples are characterized by broad (002) diffraction peaks, and their positions are much lower than the typical peak of graphite (0.3354 nm), coinciding with the low crystalline nature revealed in the HRTEM images. However, there are apparent differences between the four samples. Table 1 presents the interlayer distance values between graphene planes (d_{002}) together with the crystalline size (L_c) determined from the peak width using the Scherrer equation. P-CNT has the highest crystallinity with the narrowest d_{002} (0.34 nm) and the largest L_c (4.0 nm), whereas A-CNT has the broadest d_{002} (0.36 nm) and the smallest L_c (2.0 nm). Similar to the Raman spectra, the double coaxial CNTs (PA- and AP-CNT) have the intermediate d_{002} and L_c values between P- and A-CNT.

3.6. Fwhm of the sp^2 Carbon Peak in XPS. Each C_{1s} XPS of the carbon-coated AAO films and CNTs is characterized by a large peak around 285 eV together with a very weak shoulder on its high-energy side. The large peak can be attributed to the sp^2 carbon atoms of the carbon skeleton. Table 1 also shows that the fwhm values of the sp^2 carbon peaks have varied values among all the samples including the carbon-coated AAO films and CNTs. The fwhm value of AP/AAO is similar to those of PA- and P-CNT. The fwhm values of the other three samples (PA/AAO, AP-, and A-CNT) are also similar to each other.

3.7. Oxygen Chemisorption. The double coaxial and single-stacked CNTs were subjected to oxygen chemisorption at 200 °C just after the heat treatment under a He flow at 800 °C. The resultant chemisorbed oxygen was allowed to desorb as CO_2 and CO gases during the subsequent TPD process. As revealed in Table 1, A-CNT desorbs much larger

amounts of CO_2 and CO than the other three samples do, and P-CNT has the lowest desorption amounts of CO_2 and CO. The amounts of CO_2 and CO evolved from PA- and AP-CNT are between P- and A-CNT.

3.8. Electrical Conductance. $I-V$ characteristics for all the carbon-coated AAO films are of ohmic nature, and the resistances of these coated AAO films were obtained from each slope of the $I-V$ curves. Accordingly, the resistivity of the resultant CNTs was calculated. Table 1 shows that, among the four samples, the undoped P-CNT has the highest while A-CNT has the lowest electrical resistivity. It is apparent that the resistivity is related to the N fraction, and with the increase of N content, the resistivity decreases.

4. Discussion

The previous study proved that both the first- and the second-step CVD processes lead to the uniform deposition of carbon layers in the narrow channels of AAO template and PA-CNT is composed of outer undoped and inner N-doped multiwalls while AP-CNT is, in the reverse case, of the outer N-doped and inner undoped multiwalls.[16] The wall thicknesses of P- and PA- and A- and AP-CNT are 2.5 and 4.4 nm and 1.7 and 3.3 nm, respectively. The SEM images (Figure 4) show that the CNTs exist in bundles even after removing AAO templates, and the carbon coated on the outer surface of AAO in CVD is not destroyed and behaves as the binding agents to connect nanotubes with each other into bundle form. The N-distribution depth profiles (from upper to lower, shown in Figure 3) of PA- and AP-AAO films reveal the axial N distribution of the resultant CNTs (from inner to outer) and provide further solid proof for the formation of double coaxial CNTs. In the profile of PA-AAO, the N/C atomic ratio gradually decreases with the increase in the sputtering period, and the ratio reaches zero when the N-doped layer is fully removed and only the lower undoped layer is left. Thus, the profile gives a clear illustration of the depth-dependent N-distribution of the PA-AAO film, that is, the axial N distribution of the resultant PA-CNT. It is a little complicated in the AP-AAO case; even before the sputtering, an amount of N can be detected because the escape depth of one photoelectron is larger than the thickness of the upper layer (1.6 nm) and a little portion of the lower layer can be detected; after complete removal of the upper undoped layer, the N/C atomic ratio of AP-AAO reaches the highest level. This provides very solid proof that the resultant nanotube, AP-CNT, has a coaxial structure of outer N-doped and inner undoped multiwalls.

The elemental analysis (Table 1) provides evidence for the uniform distribution of N in the N-doped layer. For single-stack A-CNTs, their N/C surface atomic ratio (0.074), obtained from XPS, is close to that from the bulk elemental analysis (0.080). This agreement implies that N atoms are uniformly distributed in the carbon walls of A-CNT. By assumption that such a uniform distribution with an N/C ratio of 0.080 is the case also for the N-doped layers in the double coaxial CNTs, we can estimate their bulk N/C ratios only from the thicknesses of N-doped layers and undoped ones of the double coaxial CNTs. Such average ratios of PA- and AP-CNT are thus calculated to be 0.030 and 0.039, respectively, which are in accordance with those (0.030 and 0.033) determined by the elemental analysis. This finding indicates that N atoms are uniformly distributed in the N-doped layers of all three N-doped CNTs (A-, AP-, and PA-CNT) with an approximate stoichiometry of $C_{12}N$. The previous communication discussed N_{1s} spectra of PA/AAO (inner surface of PA-CNT) and AP-CNT (outer surface).[16] Both spectra were characterized by a large peak around 401.0 and a small one around 398.4 eV, suggesting the presence of quaternary N and pyridine-type N species in the N-doped layer. This finding indicates that, no matter where N is doped (in the outer or inner layer), N exists in the similar chemical states.

The HRTEM images (Figure 5) reveal that both PA- and AP-CNT have a less-crystallized structure and show no visible interface between the layers grown in the different CVD steps. Raman (Figure 6), XRD (Figure 7), and XPS (Table 1) measurements, however, confirm that there is an apparent difference in the crystallinity between the inner and the outer layers. We compared Raman spectra and XRD patterns of single-stack A-CNT with those of P-CNT to distinguish the crystallinity of carbon layers deposited by the acetonitrile CVD and propylene one. A-CNT has much larger Raman spectrum $\Delta\nu_G$ and a broader (002) peak in the XRD pattern compared with P-CNT. Lespade et al.[19] proved that the Raman $\Delta\nu_G$ is closely related to structure regularity, and the larger the $\Delta\nu_G$, the lower the graphitization degree. Meanwhile, XRD patterns of carbon materials have been well understood and the boarder (002) peaks represent a less-crystallized structure. It is thus concluded that the acetonitrile CVD leads to a less-crystallized N-doped layer compared with the undoped one prepared by the propylene CVD. PA- and AP-CNT have the crystallinity parameters between P- and A-CNT as expected since the coaxial CNTs have both N-doped and undoped layers. By identification of the fwhm values of the XPS C_{1s} peak, more direct proofs have been obtained to make sure of the crystallinity differences between the inner layer and outer one. In Table 1, the carbon-coated AAO films and CNTs are divided into two groups: group I (AP/AAO, PA-, and P-CNT) and group II (PA/AAO, AP-, and A-CNT), according to their fwhm values. The C_{1s} spectra of group I reflect the chemical structure of the carbon layers deposited by the propylene CVD, while those of group II reflect the chemical structure of carbon layers deposited by the acetonitrile CVD. In general, the wider the width of the sp^2 carbon peak becomes, the less the degree of the graphitization.[20,21] The fwhm values of the group II are apparently larger than those of the group I, further confirming that the N-doped layer is more irregular and less crystalline than the undoped one.

Incorporation of N species imparts new active sites and structural irregularity to carbon hexagonal rings, and as a result the N-doped layer has a high reactivity compared with the undoped one. As presented above (Table 1), A-CNT has much higher oxygen chemisorption capacity than undoped P-CNT. PA- and AP-CNT have the chemisorption capacities between P- and A-CNT due to the fact that the double coaxial

(19) Lespade, P.; Al-jishi, R.; Dresselhaus, M. S. *Carbon* **1982**, *20*, 427.
(20) Takahagi, T.; Ishitani, A. *Carbon* **1984**, *22*, 43.
(21) Takahagi, T.; Ishitani, A. *Carbon* **1988**, *26*, 389.

Table 2. Resistivity of Different Carbon Materials Reported in the Literatures as Compared to the Measurements in This Paper

materials	resistivity at room temperature (ρ, Ω·cm)	ref
diamond	$\sim 10^{20}$	1
graphite	5×10^{-5}	1
metallic SWNT	$(5-7) \times 10^{-4}$	22
MWNT	$5.1-5.8 \times 10^{-6}$	23
MWNT	5.3×10^{-4} to 7.7×10^{-3}	24
B-doped MWNT	7.4×10^{-5} to 7.7×10^{-4}	24
N-doped carbon film[a]	2×10^{-1}	25
N-doped carbon film[b]	10^3-10^7	26
carbon film[c]	$\sim 10^6$	27
B-doped carbon film[d]	10^1-10^3	27
P-CNT (undoped)	1.6×10^3	this paper
A-CNT (N-doped)	2.2×10	this paper

[a] Amorphous carbon (8 at. % N) prepared by filter are deposition. [b] Carbon nitride film prepared by magnetron sputtering. [c,d] Undoped and B-doped (0.5 at. % B) carbon film by filter arc deposition.

CNTs contain not only relatively inert undoped carbon layer but also a reactive N-doped one. In other words, the double coaxial CNT possess a nanotubular structure with entirely different surface chemical activity for outer and inner layers.

As shown in Table 1, both undoped and N-doped CNTs have the electrical resistivity in the range of 2.2×10 to $\sim 1.6 \times 10^3$ Ω·cm, suggesting that all four samples are semiconductors. The electrical resistivity of P- and A-CNT and some other kinds of carbon materials are summarized in Table 2. In the common case, the less the crystallinity of the graphene sheets, the higher the resistivity. In this study, the undoped P-CNT is less crystallized than single walled carbon nanotubes (SWNT) and multiwalled carbon nanotubes (MWNTs) (listed in Table 2) employed for resistivity measurements, and hence the resistivity of P-CNT is higher than most of these CNTs. Likewise, compared with the much less crystallized carbon films, P-CNT has lower resistivity.

Also on the basis of Table 2, B or N doping lowers the resistivity of the carbon structure not only for CNTs but also for carbon films. Despite less crystallinity due to the N introduction, the resistivity of A-CNT has about two orders, and those of PA- and AP-CNTs have 1 order of magnitude lower than the undoped P-CNT (Table 1). The crystallinity is likely to be less important than N doping for the conductivity of less-crystallized CNTs such as P-CNT. It is commonly accepted that the electrical conduction in less-crystallized carbon materials (including the present undoped and N-doped CNTs) occurs by a discontinuous hopping between localized states distributed in the mobility gap near a conduction band edge or the Femi energy level.[26] The doping of N (as donors) will change the electronic structure of the carbon layer, possibly shift the Femi energy level, and increase the electron density near the conduction band to promote the hopping conductance in N-doped layer. In other words, the hopping behavior is in a different intensity for undoped or N-doped layers to result in different conductivity.

5. Conclusions

This study reports the details of the aligned CNTs, with the double coaxial structure of N-doped and undoped carbon multiwalls, prepared by the template technique. The N-doped and undoped layers of each double coaxial CNT have different crystallinity and physicochemical properties, and the N-doped layer possesses less crystal nature, higher reactivity, and electrical conductivity. In other words, the structure of the present CNTs is doubly coaxial in terms of both heteroatom distribution and crystallinity, and the double coaxial CNTs can thus provide different chemical surroundings and impart different electrical conductivity to their outer and inner layers. This study demonstrates that the template technique allows one not only to control the size of CNTs, but also to selectively dope heteroatoms into carbon multiwalls to adjust the physicochemical properties. This technique will, therefore, make it possible to realize several types of coaxial electronic heterojunctions (*pn*, *npn*, or *pnp*) inside CNTs by controllable stacking *n*-type layers (doped with electron-excess elements such as N) and *p*-type layers (undoped or doped with electron-deficient elements such as B).

Acknowledgment. We gratefully acknowledge the financial support provided by the 21st Century COE program of the Japan Society of Promotion of Science (JSPS) ("Unexplored chemistry—giant molecules and complex systems"). Dr. Q. H. Yang is also grateful for the financial support from JSPS postdoctoral fellowship (P 03282) for foreign researchers.

CM047830M

(22) Zhu, H. W.; Xu, C. L.; Wu, D. H.; Wei, B. Q.; Vajtai, R.; Ajayan, P. M. *Science* **2002**, *296*, 884.
(23) Ebbesen, T. W.; Lezec, H. J.; Hiura, H., Bennett, J. W.; Ghaemi, H. F.; Thio, T. *Nature* **1996**, *382*, 54.
(24) Wei B. Q.; Spolenak, R.; Kohler-Redlich, P.; Ruhle, M.; Arzt, E. *Appl. Phys. Lett.* **1999**, *74*, 3149.
(25) Yu, Y. H.; Chen, Z. Y.; Luo, E. Z.; Cheung, W. Y.; Zhao, J. P.; Wang, X.; Xu, J. B.; Wong, S. P.; Wilson, I. H. *J. Appl. Phys.* **2000**, *87*, 2874.
(26) Wei, J.; Hing, P. *the Solid Film* **2002**, *410*, 21.
(27) Kleinsorge, B.; Ilie, A.; Chhowalla, M.; Fukarek, W.; Milne, W. I.; Robertson, J. *Diamond Rel. Mater.* **1998**, *7*, 472.